Customer:	ESA	Document Ref.:	OMPC.ACR.MEM.018
Contract No.:	4000111836/14/I-LG	Date:	15/06/2023
		Issue:	1.2

Project:	COPERNICUS SPACE COMPONENT SENTINEL OPTICAL IMAGING MISSION PERFORMANCE CLUSTER SERVICE
Title:	Impact of the use of the TSIS solar spectrum on Sentinel-3 products
Author(s):	L. Bourg, D. Smith, S. Clerc
Distribution:	OPT-MPC, ESA, EUMETSAT
File name	OMPC.ACR.MEM.018 - i1.r2 - Impact of TSIS Solar Spectrum on Sentinel-3 products.docx

ACRI-ST
260 route du Pin Montard
06904 Sophia-Antipolis, France
Tel: +33 (0)4 92 96 75 00 Fax: +33 (0)4 92 96 71 17
www.acri-st.fr

Changes Log

Version	Date	Changes
i1.r0	17/03/2023	Initial Version
i1.r1	07/06/2023	Addressing comments from SD 17/03/2023
i1.r2	15/06/2023	Modification of final recommandations

Table of content

List of Figures

List of Tables

1 Introduction

GSICS and CEOS have recently recommended to adopt as reference Solar Irradiance Spectrum theTSIS-1 HRSR 2021 (Coddington 2021 Bhatt, 2021) while the current reference spectrum is that of Thuillier (Thuillier 2003).

This document aims at assessing the impact of adopting the TSIS-1 Solar Spectrum on the OLCI and SLSTR products.

2 References

Coddington, O. M., Richard, E. C., Harber, D., Pilewskie, P., Woods, T. N., Chance, K., et al. (2021). The TSIS-1 Hybrid Solar Reference Spectrum. Geophysical Research Letters, 48, e2020GL091709. https://doi.org/10.1029/2020GL091709

Bhatt, R.; Doelling, D.R.; Coddington, O.; Scarino, B.; Gopalan, A.; Haney, C. Quantifying the Impact of Solar Spectra on the Inter-Calibration of Satellite Instruments. *Remote Sens.* **2021**, *13*, 1438. https://doi.org/10.3390/rs13081438

Thuillier, G. & Hersé, Michel & Labs, D. & Foujols, T. & Peetermans, W. & Gillotay, Didier & Simon, Paul & Mandel, H.. (2003). The Solar Spectral Irradiance from 200 to 2400 nm as Measured by the SOLSPEC Spectrometer from the Atlas and Eureca Missions. Solar Physics. 214. 1-22. 10.1023/A:1024048429145.

3 Dataset description

3.1 Thuillier 2003

The Thuillier-2003 dataset is used as a reference for Sentinel-3 data from Phase A, after having been the reference for ENVISAT/MERIS. The spectrum extends from 199.1 to 2397.5 nm; it has variable spectral sampling (from about 0.1 to 1m depending on wavelength and excluding few data gaps) and resolution (from about 1nm in the UV-VIS to ab. Solar Irradiance at 1 UA is expressed in $mW.m^{-2}.nm^{-1}$.

3.2 TSIS-1 HSRS

The TSIS-1 Total and Spectral Solar Irradiance Sensor-1 (TSIS-1) Hybrid Solar Reference Spectrum (HSRS) provides data between 202 and 2730 nm at 0.01 to ~0.001 nm spectral resolution with uncertainties of 0.3% between 460 and 2365 nm and 1.3% at wavelengths outside that range. It is expressed in $W.m^{-2}.nm^{-1}$.

at several spectral resolutions and sampling:

1. TSIS-1 HSRS, Spectral resolution: varies; equal to that of the original high-resolution datasets, sampling: 0.001 nm
2. TSIS-1 HSRS 'p005nm', Spectral resolution: 0.025 nm (<374 nm) and 0.005 nm (≥374 nm), sampling: 0.001 nm
3. TSIS-1 HSRS 'p025nm', spectral resolution: 0.025 nm, sampling: 0.005 nm
4. TSIS-1 HSRS 'p1nm', spectral resolution: 0.1 nm, sampling: 0.025 nm
5. TSIS-1 HSRS '1nm', spectral resolution: 1 nm, sampling: 0.1 nm

The latter version, with a spectral resolution of 1nm, has been selected as the most compatible with the Thuillier 2003 dataset.

4 Irradiance comparisons

Note: the two datasets being expressed in different units, a conversion of one of the dataset is thus necessary prior to any comparison; the SI unit of TSIS ($W.m^{-2}.nm^{-1}$) has been selected.

4.1 Impact on OLCI channels

Figure 1 and Figure 2 below present the two Solar Spectra over the OLCI spectral domain. Figure 1 includes Thuillier 2003 and two versions of the TSIS-1 HSRS spectrum to highlight high resolution features. Figure 2 on the contrary restricts to the most comparable spectra: Thuillier 2003 and the 1nm resolution version of TSIS, for a better readability. The irradiance axis is log-scaled to allow distinguishing small differences over the whole range. From Figure 2 it appears that the most prominent differences can be found in the visible domain.

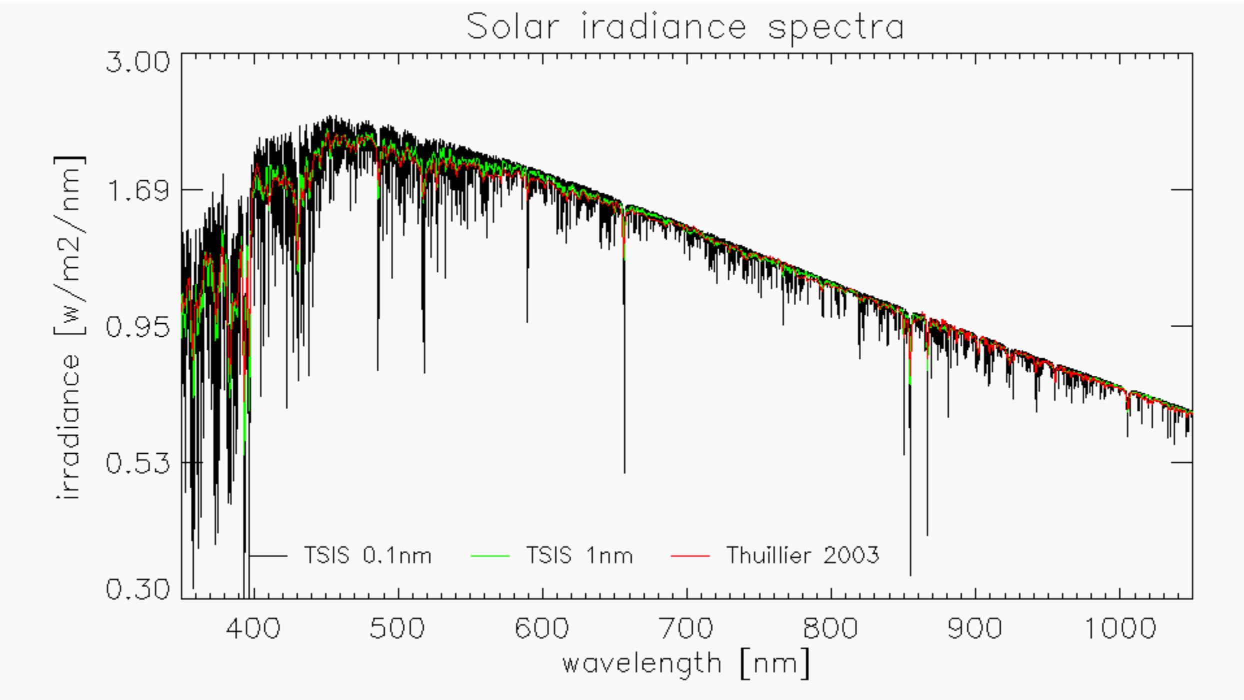

Figure 1: Thuillier-2003 and TSIS-1 HSRS (2 versions: 0.1 and 1nm spectral resolutions) over the OLCI spectral domain.

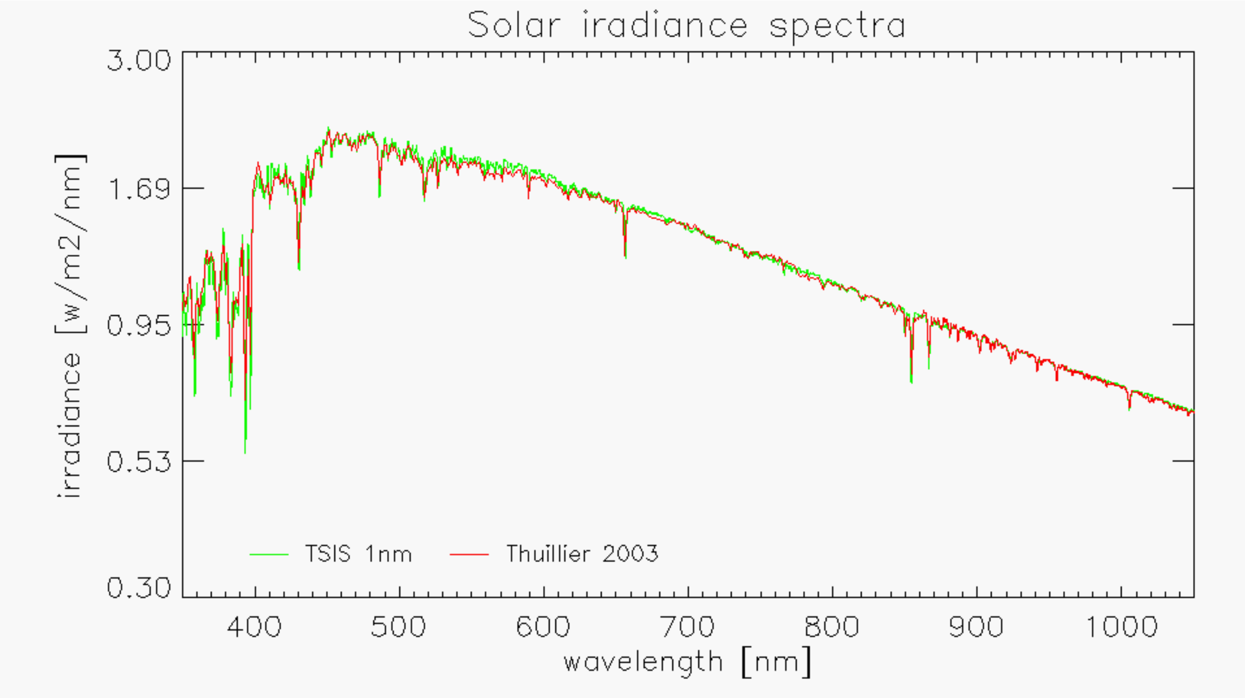

Figure 2: same as Figure 1 without the high-resolution spectrum to highlight differences.

The in-band irradiances have been computed for each OLCI channel and each Irradiance spectrum.

The in-band irradiance is the weighted mean of the Sun irradiance over the channel's SRF. It expresses as: $\frac{\int_{\lambda_1}^{\lambda_2} SRF(\lambda)\cdot E_0(\lambda)\cdot d\lambda}{\int_{\lambda_1}^{\lambda_2} SRF(\lambda)\cdot d\lambda}$ where λ_1 and λ_2 are the lower and upper limits of the SRF of the considered channel.

As the SRF and the two spectra have different spectral samplings, the irradiance spectra are first interpolated at the SRF spectral sampling. Several types of interpolation have been compared and found to be equivalent in terms of in-band irradiance.

Results using "mean" SRF for both OLCI-A and OLCI-B are shown in Table 1 below as in-band irradiance for each spectrum and relative difference in % (TSIS-1 respect Thuillier). Differences of more than 1% are highlighted in yellow if negative, in orange if positive. Relative differences are also displayed on Figure 3 to highlight high similarity of the change for the two instruments.

Table 1: In-band irradiances for OLCI-A and OLCI-B "mean" SRFs, Thuillier-2003 and TSI-1 HSRS '1nm'. Differences of more than 1% are highlighted in yellow if negative, in orange if positive.

Band	OLCI-A				OLCI-B			
	λ_c	E_0 Th.	E_0 TSIS	rDiff [%]	λ_c	E_0 Th.	E_0 TSIS	rDiff [%]
Oa01	400.30	1.513	1.459	-3.60	400.60	1.535	1.478	-3.65
Oa02	411.85	1.704	1.765	3.59	411.95	1.706	1.767	3.62
Oa03	442.96	1.889	1.899	0.50	442.99	1.890	1.899	0.49
Oa04	490.49	1.935	1.951	0.82	490.40	1.933	1.949	0.81
Oa05	510.47	1.926	1.955	1.53	510.40	1.927	1.956	1.51
Oa06	560.45	1.796	1.854	3.25	560.37	1.797	1.855	3.25
Oa07	620.41	1.649	1.678	1.76	620.28	1.649	1.678	1.78
Oa08	665.28	1.530	1.551	1.32	665.13	1.531	1.551	1.32
Oa09	674.03	1.495	1.519	1.64	673.87	1.495	1.520	1.62
Oa10	681.57	1.469	1.495	1.77	681.39	1.470	1.496	1.78
Oa11	709.12	1.403	1.399	-0.29	708.98	1.404	1.400	-0.31
Oa12	754.18	1.266	1.255	-0.88	754.03	1.266	1.256	-0.85
Oa13	761.73	1.247	1.236	-0.85	761.56	1.247	1.237	-0.84
Oa14	764.83	1.239	1.223	-1.29	764.69	1.240	1.224	-1.26
Oa15	767.92	1.230	1.210	-1.63	767.82	1.230	1.210	-1.65
Oa16	779.26	1.174	1.187	1.11	779.08	1.175	1.187	1.07
Oa17	865.43	0.960	0.955	-0.47	865.27	0.960	0.955	-0.48
Oa18	884.31	0.931	0.927	-0.44	884.13	0.931	0.927	-0.46
Oa19	899.31	0.896	0.898	0.21	899.12	0.896	0.898	0.23
Oa20	938.97	0.826	0.826	-0.09	938.80	0.827	0.826	-0.09
Oa21	1015.80	0.700	0.703	0.53	1015.74	0.700	0.703	0.53

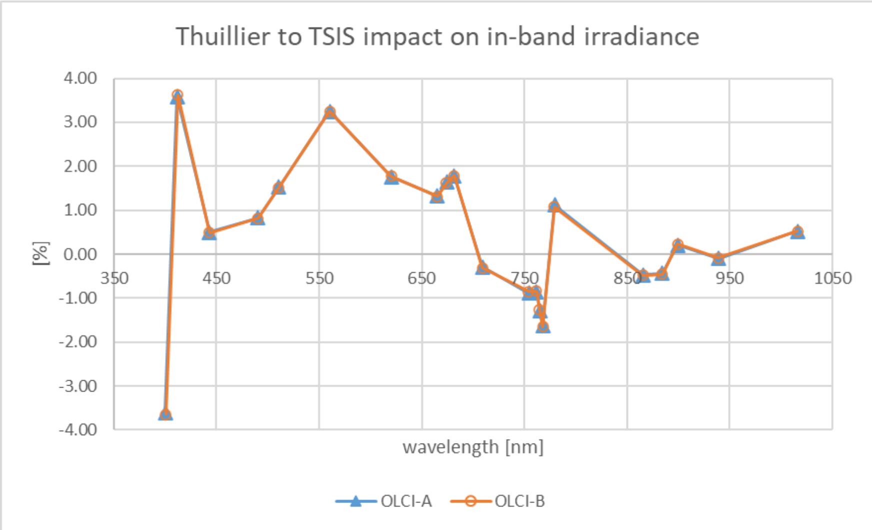

Figure 3: Impact on in-band irradiances of changing from Thuillier-2003 to TSIS-1 HSRS, for both OLCI-A (blue) and OLCI-B (orange)

As OLCI SRFs vary significantly within the field-of-view (FOV, see Figure 4), the same exercise has been repeated including a subset of the OLCI SRFs at spatial pixels. This is presented on Figure 5 for OLCI-A (left) and OLCI-B (right). The figure clearly shows that the in-FOV spectral differences have a small impact on the change.

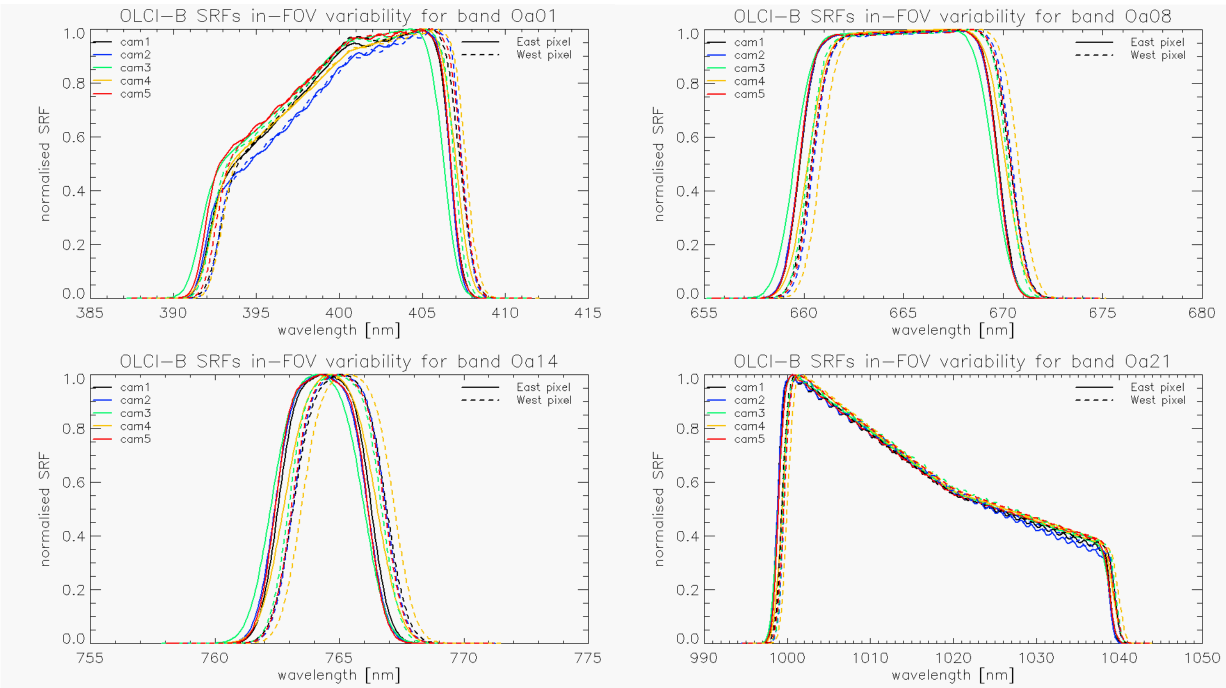

Figure 4: OLCI-B SRFs in-FOV variability for bands Oa01 (top left), Oa08 (top right), Oa14 (bottom left) and Oa21 (bottom right). SRFs are plotted for each camera (black to red colour) and for two pixels close to the camera edges (solid or dashed line).

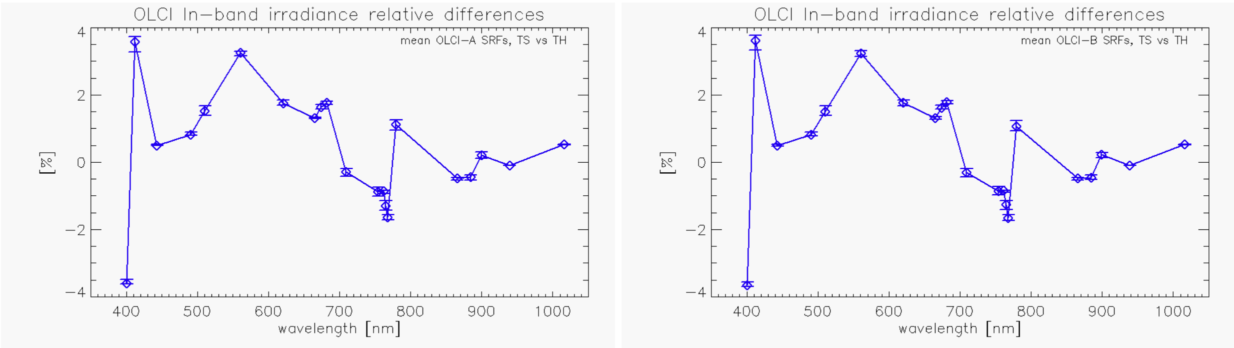

Figure 5: Impact on in-band irradiances of changing from Thuillier-2003 to TSIS-1 HSRS, for both OLCI-A (left) and OLCI-B (right). Symbols are obtained from "mean" SRFs while in-FOV variability is represented as error bars with minimum and maximum values over the FOV.

The following figures present, for each of the 21 OLCI channels, the two irradiance spectra, TSIS-1 HRS '1nm' and Thuillier 2003, over a spectral range encompassing the channel's mean SRF (Spectral Response Function) as provided on Sentinel-3 online; the SRF itself (scaled to the figure) and the corresponding in-band irradiances computed from the two spectra. The interpolated versions of the spectra are also plotted as solid lines while the original samples are plotted as symbols. Examples in Figure 6 to Figure 26 below show OLCI-A mean SRFs, but as shown by Figure 3 and Figure 5, using different SRFs would give similar results.

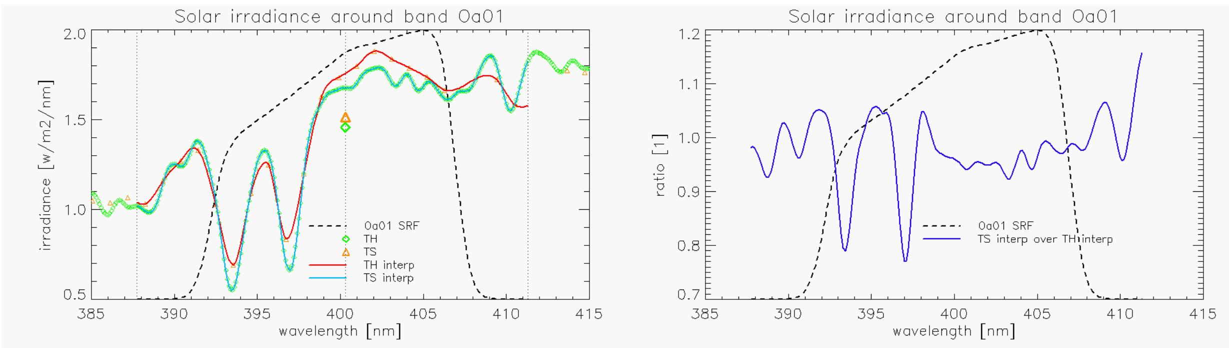

Figure 6: Left: original (symbols) and interpolated (solid lines) irradiance spectra over a spectral domain encompassing OLCI-A mean Oa01 SRF (blacked dashed line). TSIS-1 are in orange and red, Thuillier in green and cyan. Big symbols are the corresponding in-band irradiances. Vertical dotted lines mark the SRF's limits and barycentre (central wavelength). Right: ratio of the interpolated irradiance spectra over the same spectral domain (blue solid line), and mean SRF (black dashed line).

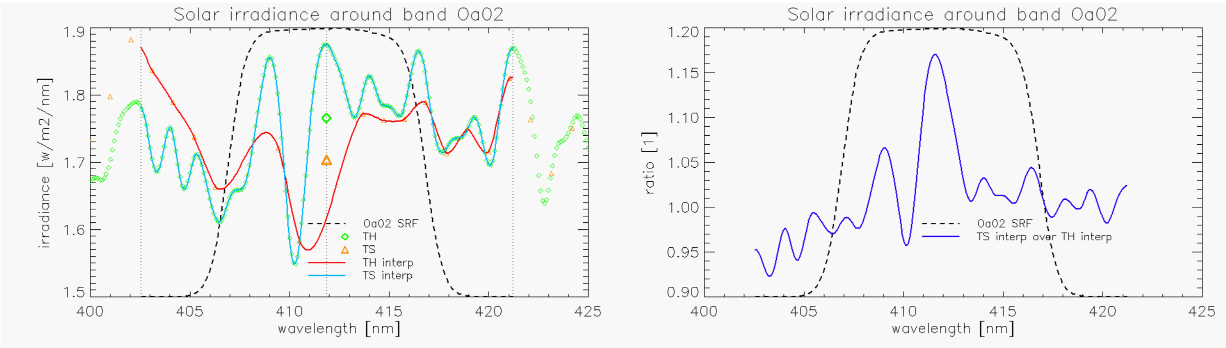

Figure 7: Same as Figure 6 for Oa02.

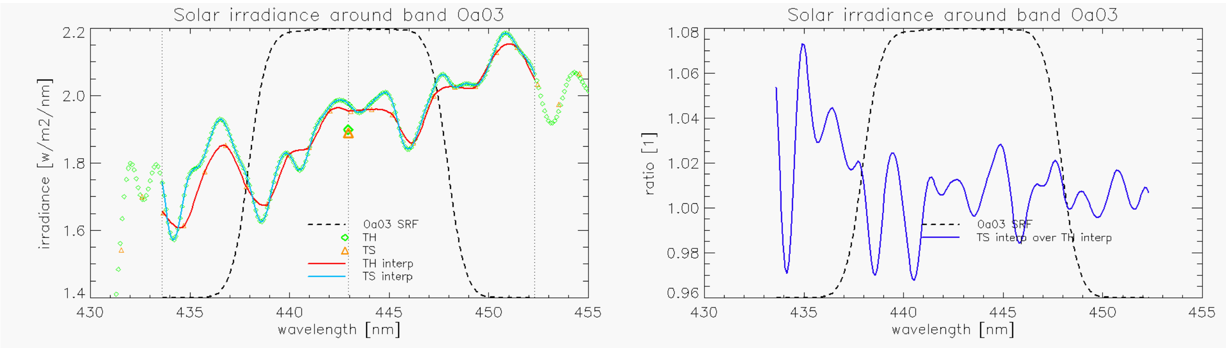

Figure 8: Same as Figure 6 for Oa03.

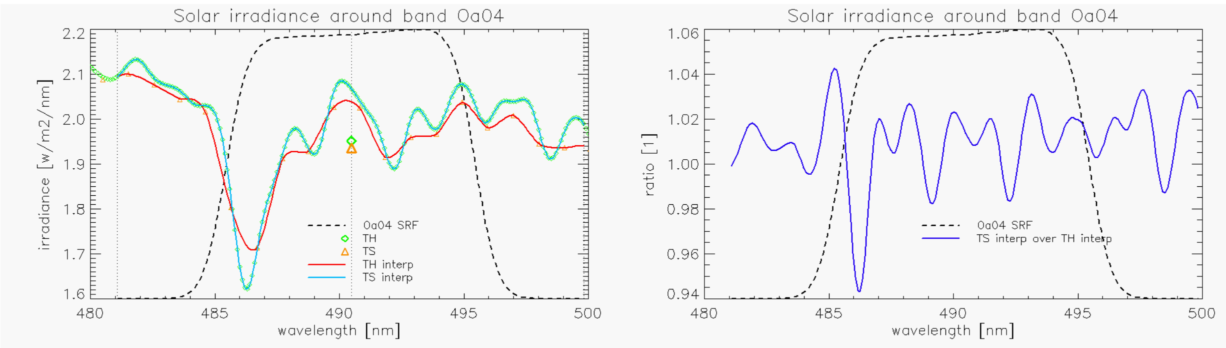

Figure 9: Same as Figure 6 for Oa04.

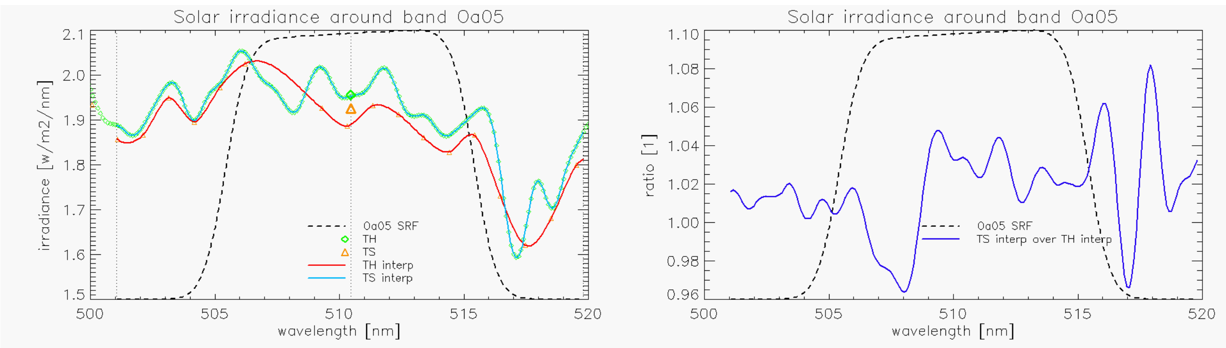

Figure 10: Same as Figure 6 for Oa05.

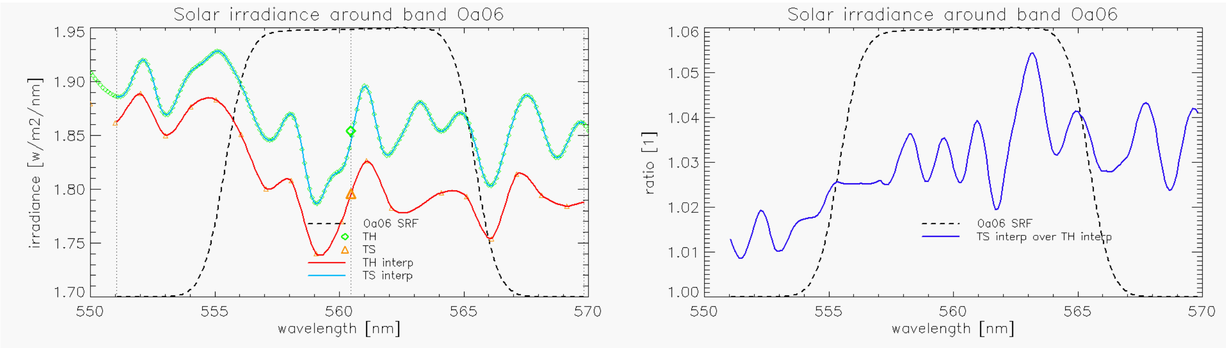

Figure 11: Same as Figure 6 for Oa06.

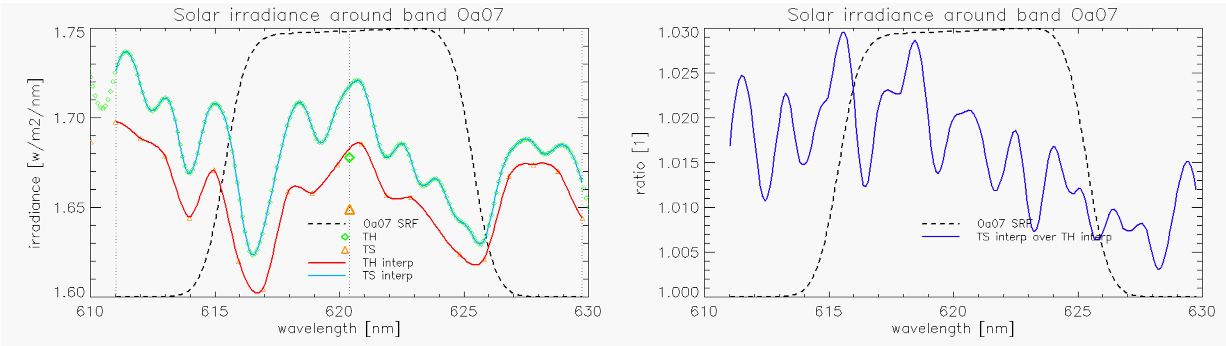

Figure 12: Same as Figure 6 for Oa07.

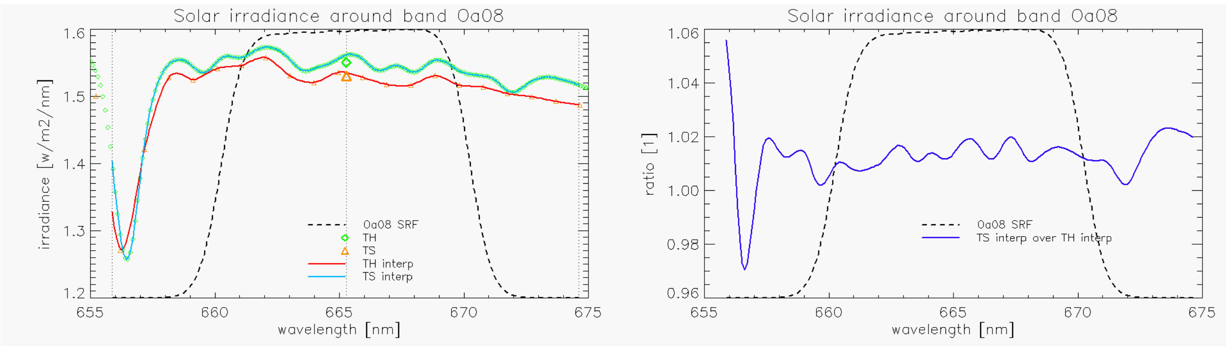

Figure 13: Same as Figure 6 for Oa08.

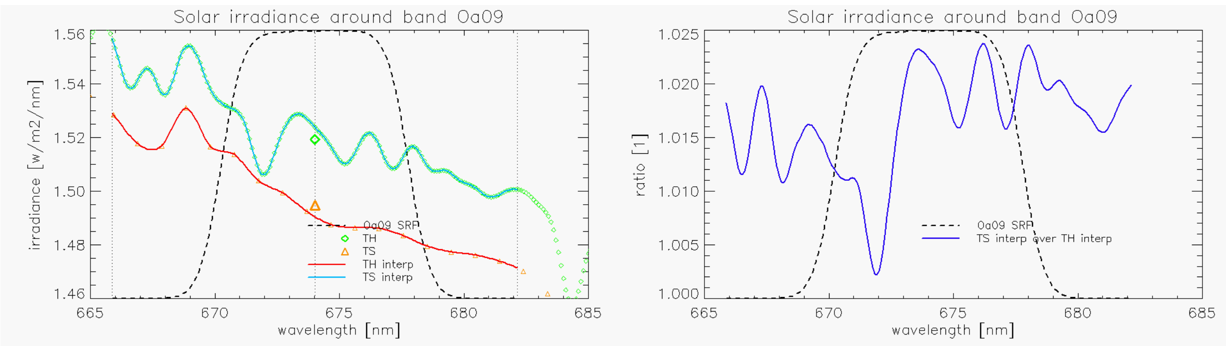

Figure 14: Same as Figure 6 for Oa09.

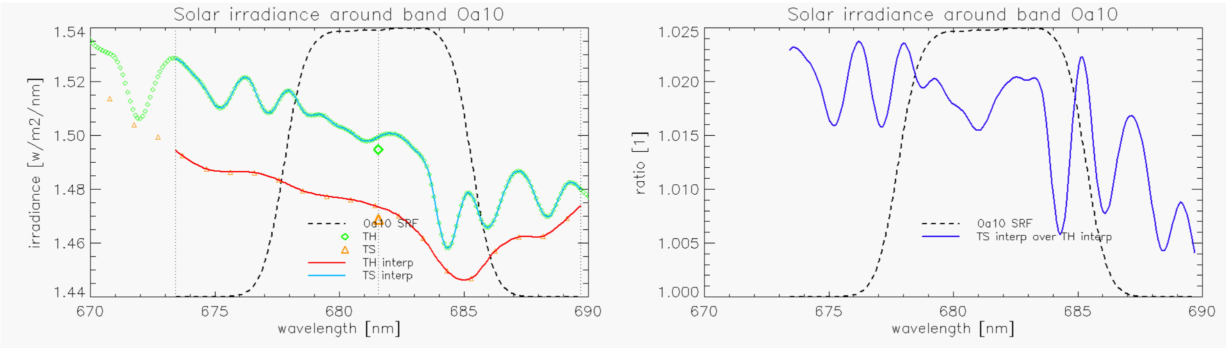

Figure 15: Same as Figure 6 for Oa10.

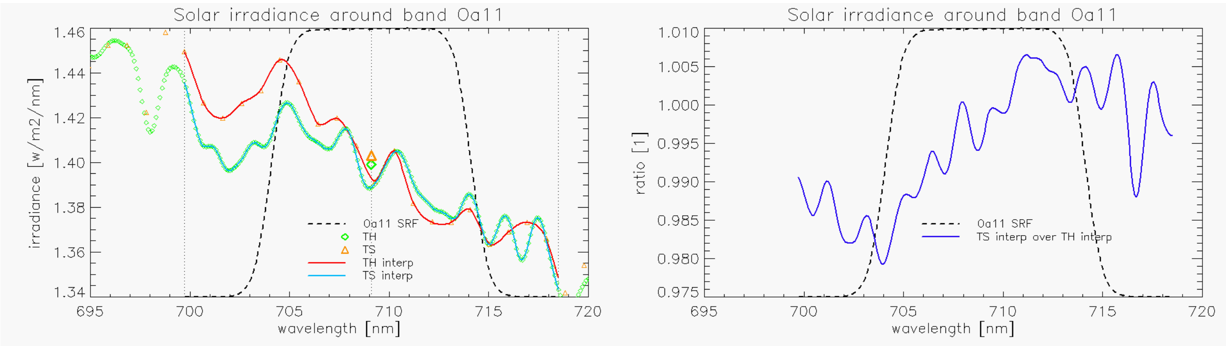

Figure 16: Same as Figure 6 for Oa11.

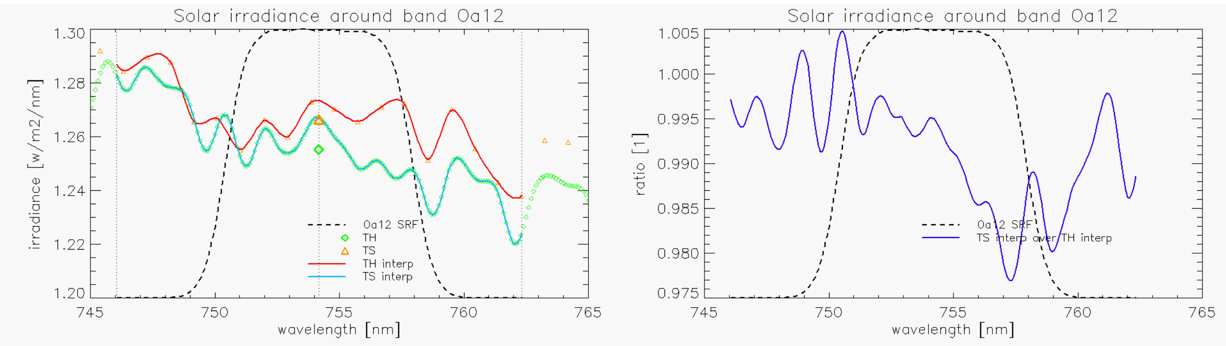

Figure 17: Same as Figure 6 for Oa12.

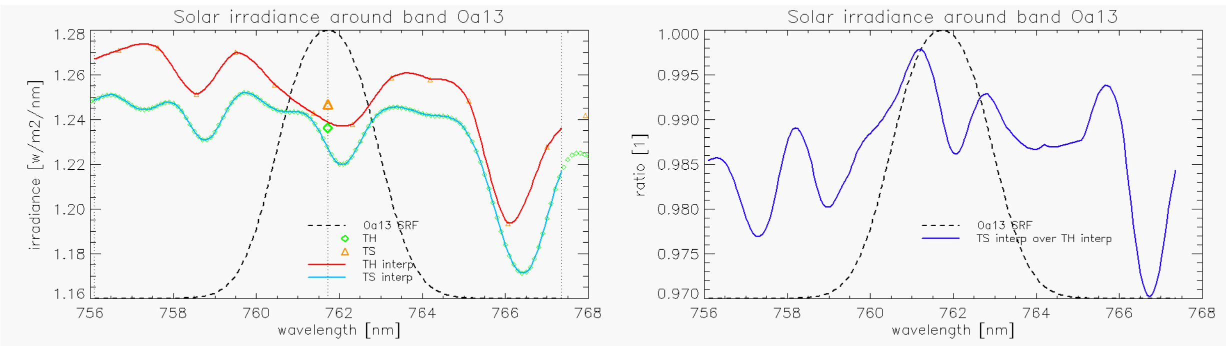

Figure 18: Same as Figure 6 for Oa13.

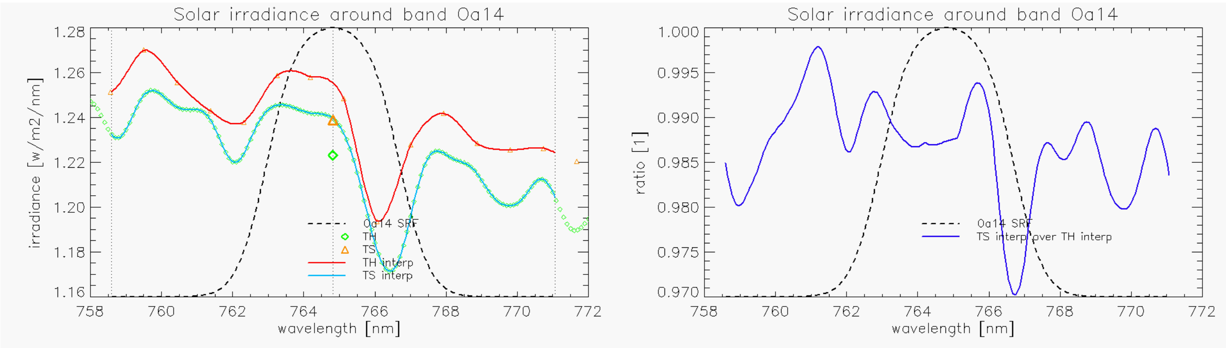

Figure 19: Same as Figure 6 for Oa14.

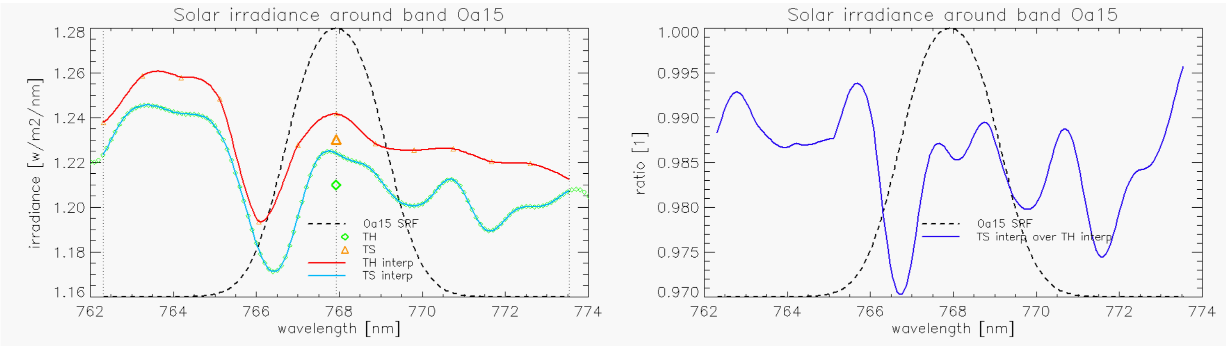

Figure 20: Same as Figure 6 for Oa15.

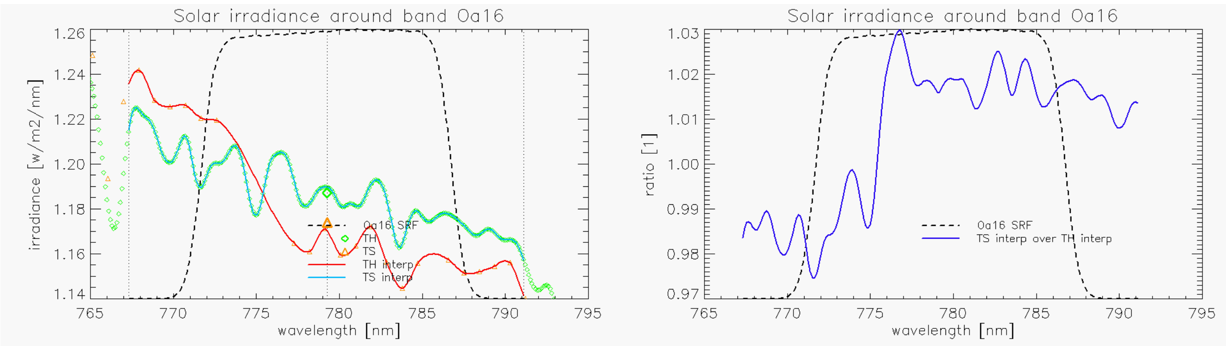

Figure 21: Same as Figure 6 for Oa16.

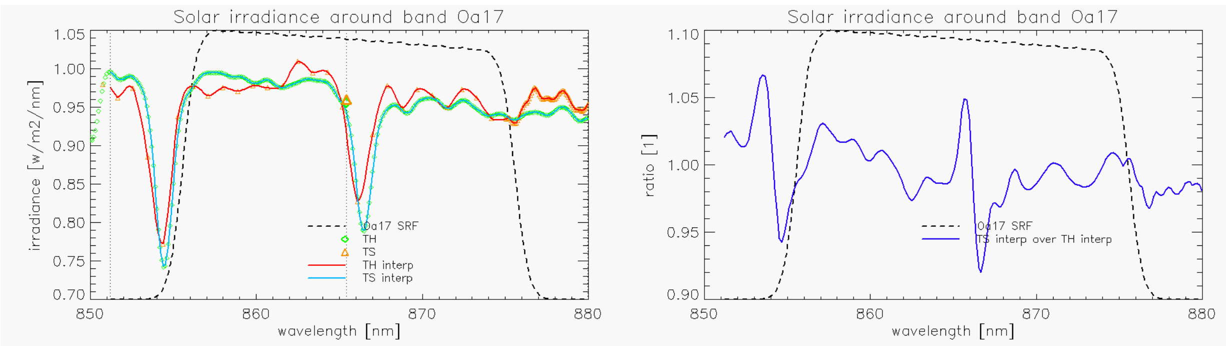

Figure 22: Same as Figure 6 for Oa17.

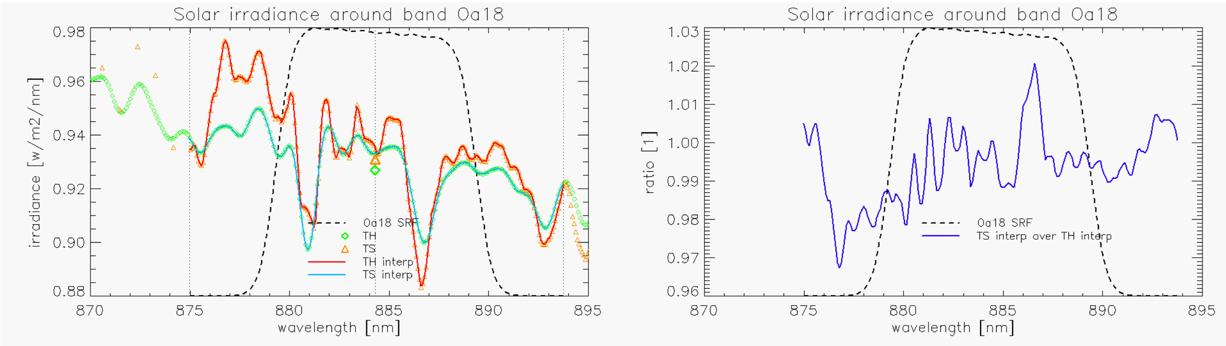

Figure 23: Same as Figure 6 for Oa18.

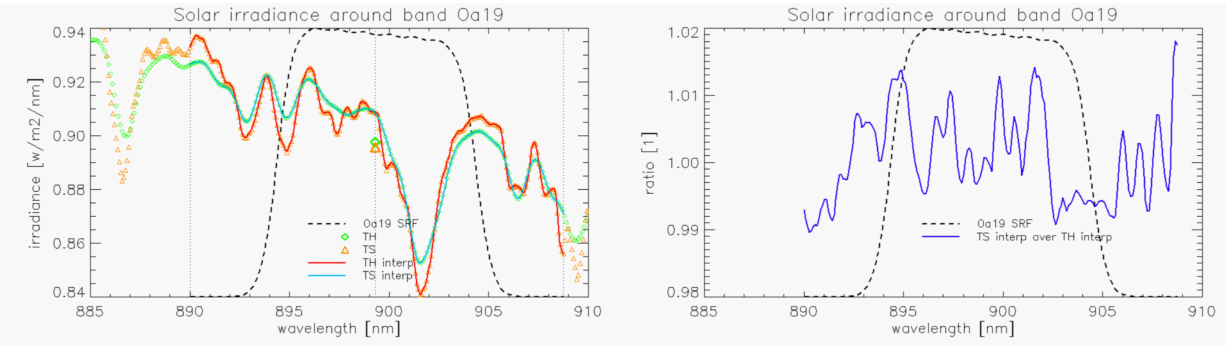

Figure 24: Same as Figure 6 for Oa19.

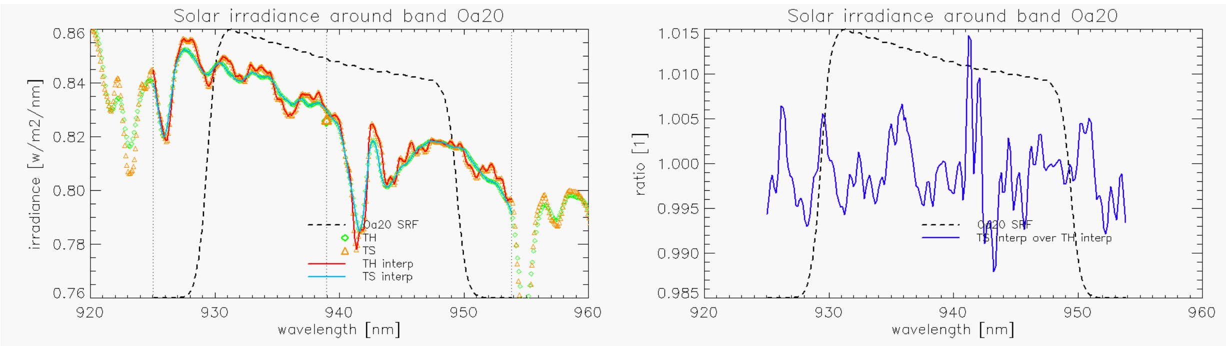

Figure 25: Same as Figure 6 for Oa20.

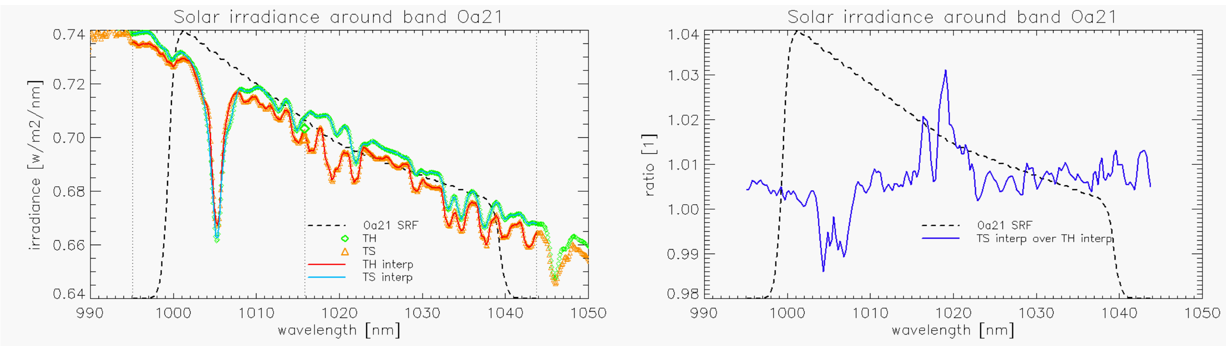

Figure 26: Same as Figure 6 for Oa21.

4.2 Impact on SLSTR solar channels

The following figure shows the position of the SLSTR solar spectral bands overlayed with the TSIS solar spectrum.

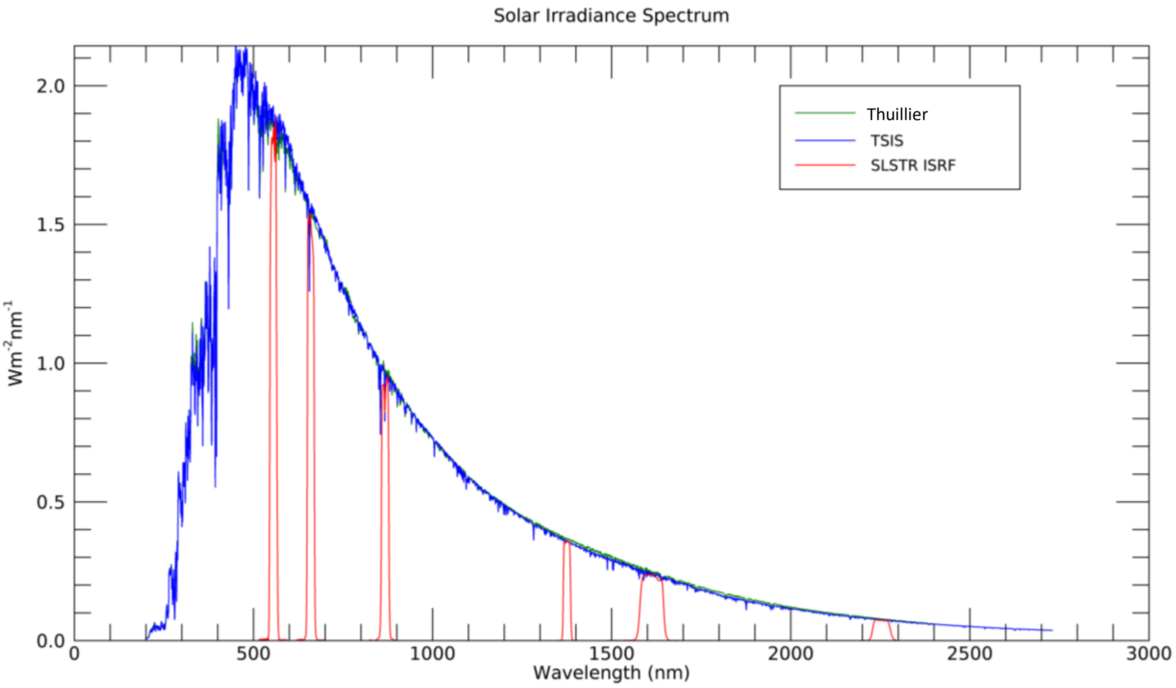

Figure 27: Thuillier and TSIS spectra overlayed on SLSTR solar channels.

The impact on the integrated solar radiance is reported in the following table:

Table 2: Impact of TSIS on solar irradiances of SLSTR channels. Yellow background indicates impact lower than −1%, Orange higher than +1%

Band	Wavelength (nm)	E_0 Thuillier ($Wm^{-2}nm^{-1}$)	E_0 TSIS ($Wm^{-2}nm^{-1}$)	Rel. Difference (%)
S1	555	1.8328	1.8767	2.39
S2	659	1.5208	1.5391	1.21
S3	865	0.9588	0.9523	-0.68
S4	1375	0.3661	0.3577	-2.30
S5	1609	0.2462	0.2377	-3.48
S6	2250	0.0779	0.0747	-4.13

5 Impact on OLCI products

5.1 Use of solar irradiance in the processing chain

Solar irradiance is used at several steps of the OLCI data processing chain.

1. Solar irradiance – in the form of in-band irradiance at each spatial pixel and channel – is an input of the Radiometric Calibration processing as one of the components of the calibration radiance computation.
2. The same in-band irradiance is also an input to the EO Level 1b processing, but only as an ancillary dataset. It is corrected for the Sun-Earth distance at the time of EO data acquisition and appended to the Level 1b product, allowing correct computation of TOA reflectance.
3. One of the very first steps of the OLCI Level 2 processing is to compute TOA reflectances from level 1 b radiances, and for this the in-band irradiances appended to the Level 1b product are used.

5.2 Impact on Level 1b

At first order, the influence of the solar irradiance change applies as a scaling factor on the radiometric gains, hence on the calibrated radiances since:

$G = \frac{X_{cal}^{corr}}{L_{cal}+SL(L_{cal})}$ (1) and $L_{EO} + SL(L_{EO}) = \frac{X_{EO}^{corr}}{G} = \frac{X_{EO}^{corr}}{X_{cal}^{corr}} \cdot (L_{cal} + SL(L_{cal}))$ (2)

Where Lcal is computed from the selected solar irradiance model and the solar diffuser BRDF model, based on ground characterisation: $L_{cal}(b) = BRDF(b) \cdot E_0(b) \cdot \cos(\theta_S)$ (3)

The fact that the irradiance change is coloured implies that it has an impact on at least the spectrometer straylight, but the straylight contribution being considered as an epsilon (see OLCI Level 1b ATBD) assumes that a change of few percent in the interband calibration should have a minor impact, so that the total impact of the irradiance change reduces to $\frac{L_{EO}^{TS}(b)}{L_{EO}^{TH}(b)} = \frac{L_{cal}^{TS}(b)}{L_{cal}^{TH}(b)} + o(SL) = \frac{E_0^{TS}(b)}{E_0^{TH}(b)} + o(SL)$ (4).

In the same way, the impact of the irradiance change on radiometric calibration takes place in the computation of the calibration radiance, with a similar impact on the spectrometer straylight computation. According to equations (1) and (3) above the gain ratio comes as: $\frac{G^{TS}(b)}{G^{TH}(b)} = \frac{L_{cal}^{TH}(b)}{L_{cal}^{TS}(b)} + o(SL) = \frac{E_0^{TS}(b)}{E_0^{TH}(b)} + o(SL)$ (5)

The exercise has been performed to run the same radiometric calibration using Thuillier-based in-band solar irradiances (reference) and TSIS-based (test). The two sets of inverse gains obtained have been ratioed and this ratio compared to the ratio of in-band irradiances to assess the straylight induced nonlinear residual. Results, averaged over the field-of-view, are displayed on Figure 28. One can see that (a) the ratio of inverse gains is visually identical to the ratio of irradiance and (b) there are some residual differences but around two orders of magnitude lower. On Figure 28 the residuals due to straylight are expressed as the relative difference between the ratio of inverse gains and the ratio of irradiance in %: $100 \cdot \left(\frac{G^{TH}(b)}{G^{TS}(b)} \Big/ \frac{E_0^{TS}(b)}{E_0^{TH}(b)} - 1 \right)$, and appear very small. However, the profiles of $\frac{G^{TH}(b)}{G^{TS}(b)} \Big/ \frac{E_0^{TS}(b)}{E_0^{TH}(b)}$ show spectral and spatial structures; spectral structures are roughly linear with the spectral irradiance changes, spatial structures, mostly visible for bands 1 and 2 – are typical of the straylight signature, increasing toward camera edges (Figure 29). Values are within 0.01% for most bands and can reach 0.08% for band Oa01 (worst case, peak).

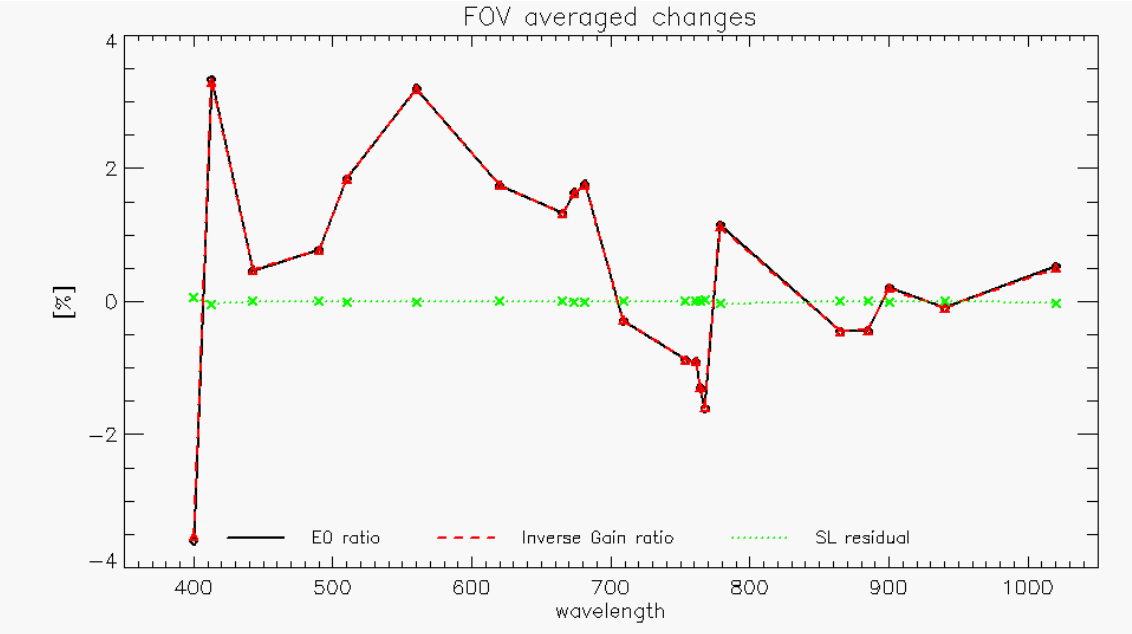

Figure 28: ratios of in-band irradiance (black solid line and diamonds), inverse gains (red dashed line and triangles) and residuals (green dotted line and X).

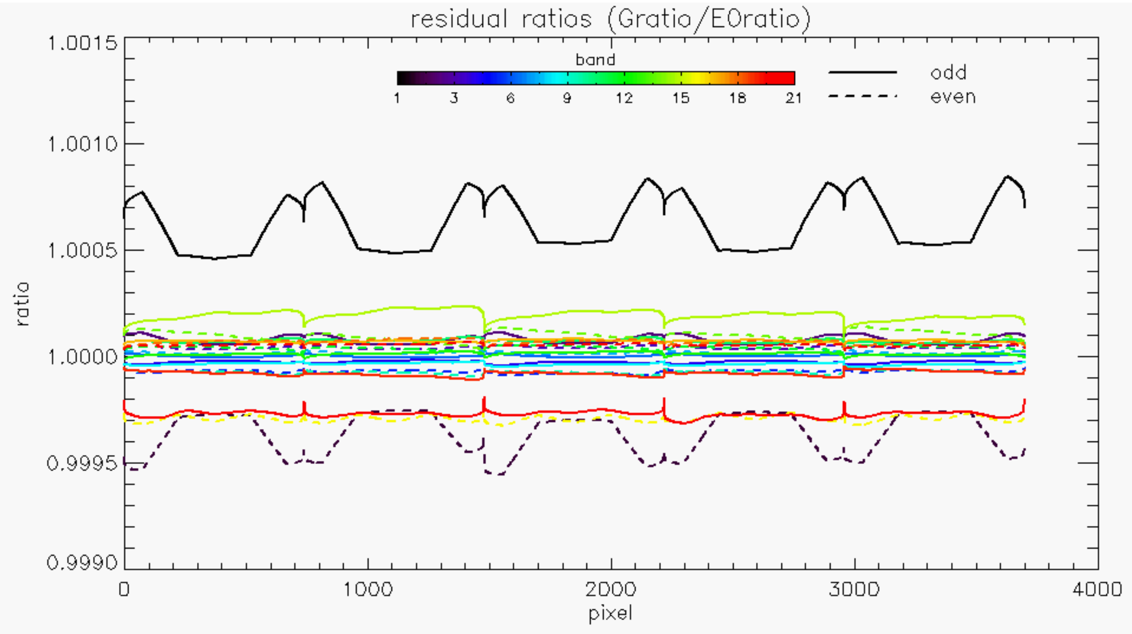

Figure 29: non-linear residuals introduced by the straylight in the radiometric gain computation.

As a general conclusion, one can thus consider that, by and large, the changes to Level 1b radiances will be a direct transposition of the in-band irradiance changes presented in Table 1, Figure 3, and Figure 5.

5.3 Impact on Level 2

All Level 2 products are computed from TOA reflectance and, considering that the in-band irradiance $E_0(b)$ is contained in the Level 1b product, the change should be totally transparent.

On the other hand, re-computation of some parameters or look-up-tables based on radiative transfer may have an impact under certain conditions.

5.3.1 OTCI

The only potential influence would be the parameters and LUTs used in the Rayleigh correction, providing they were computed with integration over a bandwidth and not as monochromatic quantities. To our knowledge, these parameters – inherited from MERIS – have been computed as monochromatic quantities with unit solar flux.

5.3.2 GIFAPAR

The various parameters involved in the GIFAPAR retrieval have been computed using OLCI-A mean SRF with an unknown reference E_0 spectrum. The source of the spectrum is under verification at JRC.

6 Impact on SLSTR products

6.1 Impact on L1b products

As for OLCI, the L1b solar channels are calibrated in reflectance and converted to radiance using the reference solar spectrum. Therefore, there is a direct impact of the choice of the spectrum on radiance measurements.

There is no impact on thermal channels which are calibrated in radiance using the on-board Black Bodies.

6.2 Impact on Level 2 products

All L2 products which rely on reflectances of solar channels are not impacted by the choice of the solar spectrum provided that the correct solar irradiances are used.

On the other hand the Fire Products rely on thresholds on SWIR channel radiances (not reflectances). We list below the different occurrences.

6.2.1 Night-time fire detection

ATBD (issue 5.0 Feb 2021) chapter 3.2.4.1 equation (17c) used for night-time fire detection:

$$\left[L_{S6} > \left(\mathrm{p}_1 + \bar{L}_{S6} + (\mathrm{p}_2 \times n_{S6})\right)\right] \text{ AND } (L_{S6} > \mathrm{p}_3) \qquad \text{for night pixels only}$$

Where $\mathrm{p}_1 = 0.03\ \mathrm{mW \cdot m^{-2} \cdot sr^{-1} \cdot nm^{-1}}$, $\mathrm{p}_2 = 2$, and $\mathrm{p}_3 = 0.25\ \mathrm{mW \cdot m^{-2} \cdot sr^{-1} \cdot nm^{-1}}$

$$\left[L_{S5} > \left(\mathrm{p}_1 + \bar{L}_{S5} + (\mathrm{p}_2 \times n_{S5})\right)\right] \text{ AND } (L_{S5} > \mathrm{p}_3) \qquad \text{for night pixels only (17d)}$$

Where $\mathrm{p}_1 = 0.05\ \mathrm{mW \cdot m^{-2} \cdot sr^{-1} \cdot nm^{-1}}$, $\mathrm{p}_2 = 2$, and $\mathrm{p}_3 = 0.24\ \mathrm{mW \cdot m^{-2} \cdot sr^{-1} \cdot nm^{-1}}$

These equations are also directly impacted by a change of solar reference spectrum and therefore need to be adapted.

6.2.2 SWIR-based FRP retrieval

ATBD (issue 5.0 Feb 2021) chapter 3.3.7.2 equation (23) SWIR radiance method for FRP retrieval appropriate for gas flares (high temperature):

$$FRP_{SWIR} = \frac{A_{sampl}}{10^6 \times t_{SWIR}} \left(\frac{s}{p}\right) \left(L_{SWIR} - L_{b,SWIR}\right)$$

Where p = 6.1 x 10^{-9} $\mathrm{W \cdot m^{-2} \cdot sr^{-1} \cdot \mu m^{-1} \cdot K^{-4}}$, and A_{sampl} is the ground projection area of the sensor FOV (in m^2).

The same conclusion applies.

7 Impact on SYN products

7.1 SYN L2 products

All computations in the SYNERGY processing are performed in reflectances. Therefore a change of solar spectrum would not have any impact as long as radiances and E_0 irradiances are consistent in the L1 product.

7.2 SYN VGT products

To interpolate the Sentinel-3 products on the PROBA-V spectral channels, a high-resolution spectrum is constructed by interpolating data from OLCI and SLSTR channels. This computation is performed on (top-of-atmosphere) reflectances. It is not impacted by a change of reference solar spectrum.

8 Recommendations

8.1 Current Sentinel-3 Products

As explained above, the impact of a change of solar spectrum would have a relatively strong impact on radiances in L1 products. However, L2 products would be mostly unaffected as most computations are performed using reflectances (a notable exception is the SLSTR FRP SWIR-based fire detection).

The OPT-MPC therefore recommends switching to the TSIS reference spectrum for current Sentinel-3 products only when a full-mission reprocessing can be undertaken in parallel.

The OPT-MPC also recommends to further investigate the impact of the change on SLSTR FRP and SWIR-based fire detection.

Additionally, conversion factors should be made available to users for inter-operability with other radiance measurements. The conversion factors from Table 1 and 2 could be displayed on Sentinel on-line web pages. In addition, a spreadsheet providing per-pixel conversion factors for OLCI should be provided. When the switch to TSIS is done, backward conversion factors shall also be provided to users.

8.2 Optical-S3 Next Generation

The use of the TSIS solar spectrum is recommended for S3 Next Generation radiance products.

End of document